ELSEVIER

Journal of Nuclear Materials 265 (1999) 232–239

journal of nuclear materials

Effects of thermal sensitization on radiation-induced segregation in type 304 stainless steel irradiated with He-ions

O. Okada *, K. Nakata, S. Kasahara

Nuclear Plant Materials Group, Hitachi Research Laboratory, Hitachi Ltd., Second Department of Materials Research, Hitachi-shi, 1-1 Saiwai-cho-3-chome, Ibaraki-ken 317-8511, Japan

Received 17 August 1988; accepted 4 November 1998

Abstract

Type 304 stainless steels, solution-annealed and thermally sensitized at 923 K for 0.5 to 24 h, were He-ion-irradiated up to about 4 dpa at 723 K and radiation-induced segregation (RIS) at grain boundaries was measured by EDS analysis using a FEG-TEM. Ni, Si and P were enriched, and Cr was depleted at the grain boundaries by irradiation. However, although the irradiation dose was the same for the specimens, the RIS of the elements linearly increased with the logarithm of the thermally sensitizing time, except for Cr in the specimen thermally sensitized for 24 h. The enhancement of RIS was attributed to the radiation-induced point defects having large mobility in thermally sensitized stainless steels, because of an expected decrease in C near the grain boundaries and in the matrix after the sensitization heat treatments. It was clarified by the electrochemical potentiokinetic reactivation test (EPR) that the degree of sensitization increased with the progress of Cr depletion at grain boundaries. The Cr concentration at grain boundaries in the heavily sensitized specimen was not changed, and the width of the depleted area was slightly narrowed by the irradiation. This result could be explained that the diffusion of Cr due to initial Cr concentration gradient near grain boundaries exceeded the inverse Kirkendall effect.

1. Introduction

Particle irradiations induce solute segregation near grain boundaries in austenitic stainless steels due to migration of excess vacancies and interstitials formed by irradiation. As well known, oversized solutes, such as Cr and Mo, are depleted from grain boundaries and undersized solutes, Ni, Si and P, are enriched by irradiation. The radiation-induced segregation (RIS) increases with irradiation fluence [1–3]. The segregation is considered to influence various properties in steels. The Cr depletion is one of the most important causes of irradiation-assisted stress corrosion cracking (IASCC) [2–6]. The threshold neutron fluence of IASCC susceptibility is considered to range from 5×10^{24} to 1×10^{25} n/m^2 [7,8].

On the other hand, stainless steels containing high C are sensitized during welding and thermal aging. The sensitization is caused by formation of Cr depleted zones on grain boundaries due to precipitation of Cr carbides. Susceptibility of intergranular stress corrosion cracking (IGSCC) in high temperature water has been related to the Cr concentration at grain boundaries. In-vessel components made of stainless steels in light water reactor are usually constructed by welding, and some weld joints should suffer neutron irradiation during reactor operation. Therefore, a change in SCC susceptibility, as well as mechanical properties and swelling, caused by irradiation is practically important especially in heat affected zones (HAZ) of weld joints.

IGSCC susceptibility in type 304 stainless steels thermally sensitized at 1023 K for 100 min and followed by aging at 773 K for 24 h was reported to be enhanced by neutron irradiation to a very low dose of 3×10^{23} n/m^2 at 563 K [9]. Moreover, radiation-induced hardening along grain boundaries in the thermally sensitized specimen was larger than that in a solution-annealed one after irradiation up to 4×10^{24} n/m^2 [10]. Swelling in HAZ of electron-beam-weld joints was also larger than

* Corresponding author. Tel.: +81-294 23 5771; fax: +81-294 23 6952; e-mail: hlmgoo@hrl.hitachi.co.jp.

0022-3115/99/$ – see front matter
PII: S0022-3115(98)00733-8

that in weld metals and base metal in modified 316L stainless steel irradiated at 873 K up to 25 dpa [11].

The objective in this work is to investigate fundamentally RIS behavior near grain boundaries in thermally sensitized type 304 stainless steel, using He-ion irradiation.

2. Experimental procedures

The material used in this study was type 304 stainless steel with 0.054 wt% carbon. The chemical composition is shown in Table 1. The material was solution-annealed at 1323 K for 0.5 h. The heat treatments for sensitization were carried out at 923 K for 0.5, 7 or 24 h in vacuum followed by water quenching.

The disks for He-ion irradiation and FEG-TEM/EDS analysis, 3 mm in diameter and 0.2 mm thick, were electropolished in a solution of 95% acetic acid and 5% perchloric acid at about 290 K. The electropolished specimens were irradiated with 100 keV He-ions at 723 K up to a fluence of 3×10^{21} ions/m^2 with a flux of 8.3×10^{17} ions/m^{2}s by using a Cockcroft ion accelerator. The distributions of damage and He concentration were calculated by the TRIM-92 code. The damage and He concentration peaked at about 300 and 350 nm depths from the irradiated surface, respectively [12].

The solute compositions near grain boundaries before and after irradiation were analyzed by FEG-TEM with an EDS, operating at 200 kV. The smallest spot size and its probe current were nominally 1 nm and 0.5 nA, respectively. X-ray spectra were taken at 1–2 nm steps across the grain boundaries for 100 s each. The X-ray spectra were converted into concentrations by applying the ratio technique [13], assuming a thin foil approximation [14]. The He-ion-irradiated specimens were sputtered with Ar-ions to clean the foil surface before EDS analysis. The foil thickness in the analyzed area was about 100 nm, estimated by counting the number of equal thickness fringes from the foil edge. The average dose in the area was calculated to be 4 dpa, neglecting the surface effect. High-angle and random grain boundaries were selected for the EDS analysis, which was carried out at three different grain boundaries per specimen condition.

In order to estimate macroscopically the degree of sensitization before and after irradiation, the double-loop electrochemical potentiokinetic reactivation test (DL-EPR) was applied [15,16]. The specimens were a plate of $10 \times 10 \times 1$ mm^3, which were polished by #800 Emery paper. For this test, some specimens were irradiated with 400 keV He-ions at 723 K to a fluence of 1×10^{21} ions/m^2 with a flux of 6×10^{17} ions/m^2 s. In this case, the peak damage to be 4 dpa was located at a depth of about 800 nm from the irradiated surface. The degree of sensitization was evaluated by the reactivation ratio of the maximum anodic and reactivation current. The DL-EPR test was carried out in a solution of 0.5 mol/l H_2SO_4 and 0.01 mol/l KSCN at about 303 K while sweeping the corrosion potential at a rate of 100 mV/min.

Table 1
Chemical composition of type 304 stainless steel used (wt%)

C	Si	Mn	P	S	Ni	Cr	Fe
0.054	0.47	0.99	0.026	0.002	8.90	18.95	bal.

3. Results

Microstructures near grain boundaries before irradiation are shown in Fig. 1 for the solution-annealed specimen and the specimens sensitized at 923 K for 0.5 and 24 h. No carbides are found at grain boundaries in the solution-annealed specimen. Fine carbides can be observed at grain boundaries in the specimen sensitized at 923 K for 0.5 h; the average diameter of the carbides is 40 nm. In the specimen sensitized at 923 K for 24 h, coarse carbides, with an average diameter of 180 nm, are observed along grain boundaries. The carbides are mainly $Cr_{23}C_6$ type, as confirmed by electron diffraction and EDS analysis. Sensitizing time dependence of Cr concentration at grain boundaries is shown in Fig. 2. The EDS analysis was performed between the carbides. The Cr concentration decreases with an increase in sensitizing time; the concentration at the grain boundary goes down to 11% after sensitization for 24 h. No change in Ni and Si concentrations at grain boundaries appears from the sensitization heat treatments, but P is slightly enriched (cf. Fig. 7(a)).

Fig. 3 shows Cr and Ni profiles near a grain boundary before and after irradiation to 4 dpa at 723 K in a solution-annealed specimen. The concentration profiles reproduced here are typical examples; the three concentration profiles per specimen all show similar trends. Before irradiation, Ni and Cr concentrations at the grain boundary are the same as those in the matrix. Ni concentration at the grain boundary is increased by about 1.5% from the matrix concentration due to the irradiation. The Cr and Ni concentrations in the matrix were determined by measurements at about 200 nm from the grain boundary. Enrichment of Ni is found in an area about 10 nm wide near the grain boundary, and accompanied by a slightly depleted area. Si and P are also enriched to about 0.5% and 0.3% at the grain boundary after the irradiation. By contrast, a small Cr depletion resulting from the irradiation is observed at the grain boundary and a slight enrichment of Cr is found on both sides of the grain boundary.

Cr and Ni profiles near a grain boundary before and after irradiation are shown in Fig. 4 for the specimen

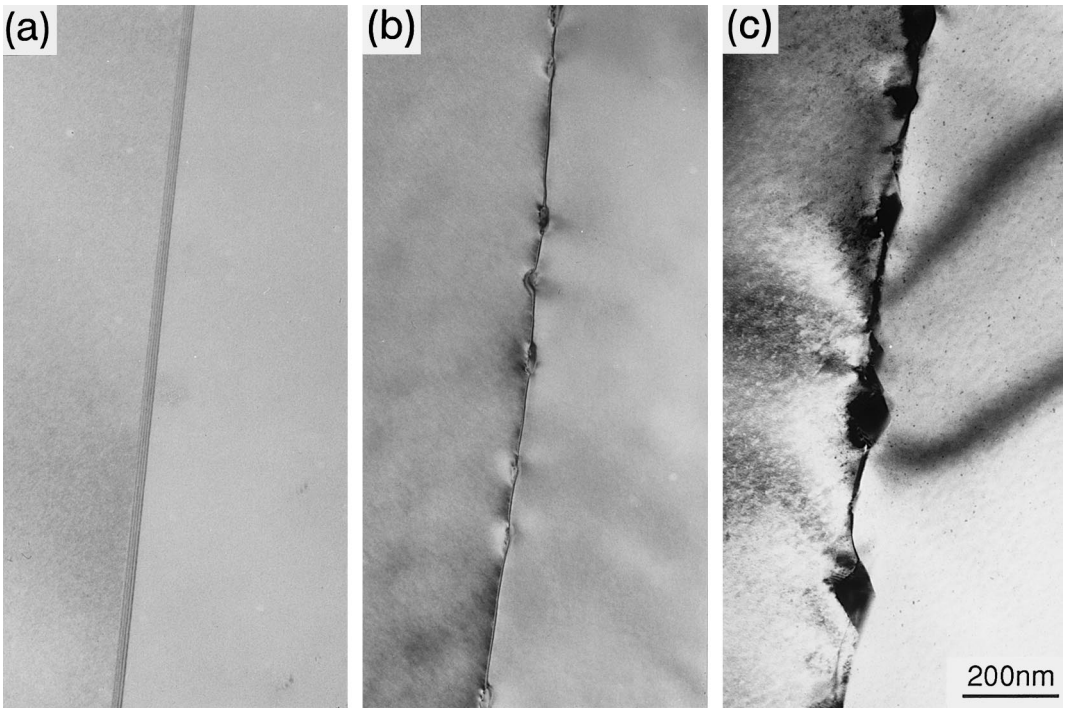

Fig. 1. Microstructures in the vicinity of grain boundaries in type 304 specimens: (a) solution-annealed; (b) sensitized at 923 K for 0.5 h; and (c) sensitized at 923 K for 24 h.

sensitized at 923 K for 0.5 h. Cr concentration at the grain boundary before irradiation is 17.5% and the depleted area has a width of about 10 nm, while there is no change in Ni concentration. The Cr depletion near the grain boundary after irradiation is deeper and wider than that in the unirradiated specimen. The Cr concentration is 16% at the grain boundary and the width of the Cr depleted area is about 20 nm. The areas, where Cr is slightly enriched, are just outside of the depleted area. Ni is enriched at the grain boundary after irradiation. The enriched area is about 5 nm in width, which is narrower than the depleted area of Cr. On the other hand, Si and P are enriched 1.3% and 0.5% at the grain boundary after irradiation. In spite of having the same

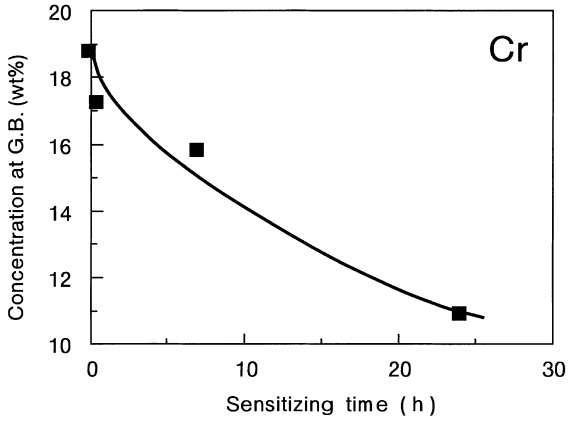

Fig. 2. Sensitizing time dependence of Cr concentration at grain boundaries (G.B.) in the specimens thermally sensitized at 923 K.

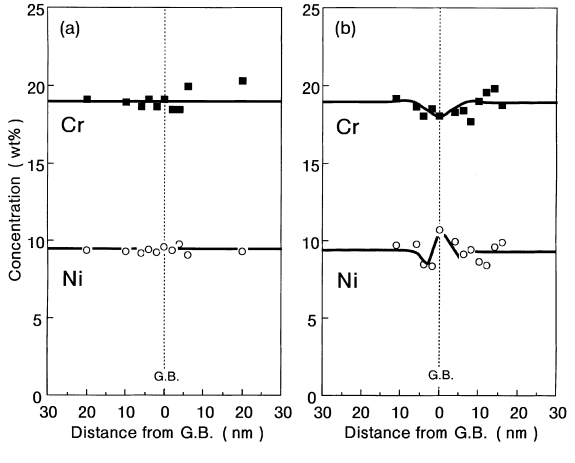

Fig. 3. Cr and Ni profiles near a grain boundary (G.B.) in the solution-annealed specimen (a) before and (b) after irradiation to 4 dpa at 723 K.

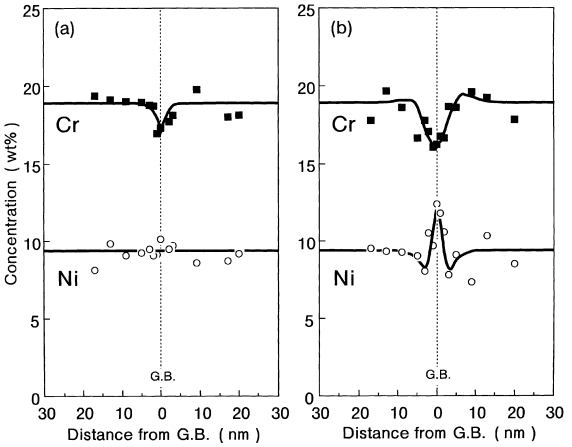

Fig. 4. Cr and Ni profiles near a grain boundary (G.B.) in the thermally sensitized specimen (923 K × 0.5 h) (a) before and (b) after irradiation to 4 dpa at 723 K.

irradiation dose, the enrichment of Ni and Si are larger than that in the solution-annealed one.

The case of the specimen thermally sensitized at 923 K for 7 h is shown in Fig. 5. After thermal sensitization, the Cr concentration falls down to about 16% at the grain boundary, but Ni concentration remains at that of the matrix. The decrease in Cr concentration at the grain boundary caused by irradiation is remarkably large, compared with that in the solution-annealed and lightly sensitized specimens. The width of the Cr depleted area is about 20 nm, which is, however, nearly the same width as the lightly sensitized specimen.

The Cr depletion near the grain boundary before irradiation is very large in the specimen heavily sensitized at 923 K for 24 h, as shown in Fig. 6(a). The minimum concentration and width of Cr depletion are 11% and 40 nm, respectively. After irradiation to 4 dpa at 723 K, the Cr concentration at the grain boundary hardly changes in comparison with the value before irradiation. The width of the Cr depleted area after irradiation is half as narrow as that before irradiation (Fig. 6(b)). However, slight enrichment of Cr appears on both sides of the depleted area, and moreover, Ni enrichment of 4.2% is found in the irradiated specimen. Si and P concentration profiles before and after irradiation are shown in Fig. 7. Si and P are also apparently enriched at the grain boundary by the irradiation. These results suggest the following: when Cr concentration at grain boundaries is lower, the concentration dose not seem to be changed by irradiation, and the width of the depleted area is narrowed by it. In other words, the Cr depletion near grain boundaries, which occurs because of thermal sensitization treatments, is somewhat recovered by irradiation in this case.

The RIS at grain boundaries is summarized in Fig. 8, as a function of the logarithm of the thermally sensitizing time. In the figure, the amount of RIS is defined as the difference between the concentrations in wt% at a grain boundary after irradiation and before it. Although the irradiation dose is the same among the specimens, the RIS of all the elements linearly increases with the logarithm of the thermally sensitizing time, except for Cr in the specimen sensitized for 24 h. The segregation of Ni is about 4% in the specimen sensitized for 24 h, which is about three times larger than that in the solution-annealed one. The RIS behavior of Cr remarkably differs with the degree of sensitization before irradiation.

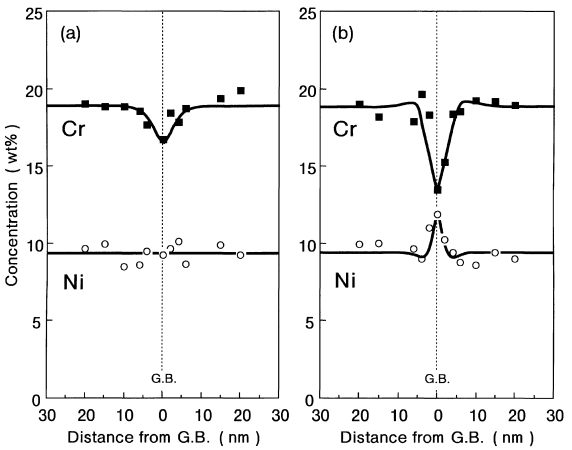

Fig. 5. Cr and Ni profiles near a grain boundary (G.B.) in the thermally sensitized specimen (923 K × 7 h) (a) before and (b) after irradiation to 4 dpa at 723 K.

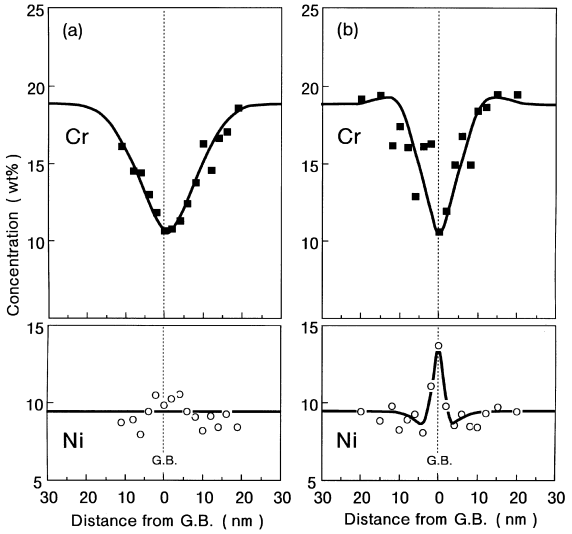

Fig. 6. Cr and Ni profiles near a grain boundary (G.B.) in the thermally sensitized specimen (923 K × 24 h) (a) before and (b) after irradiation to 4 dpa at 723 K.

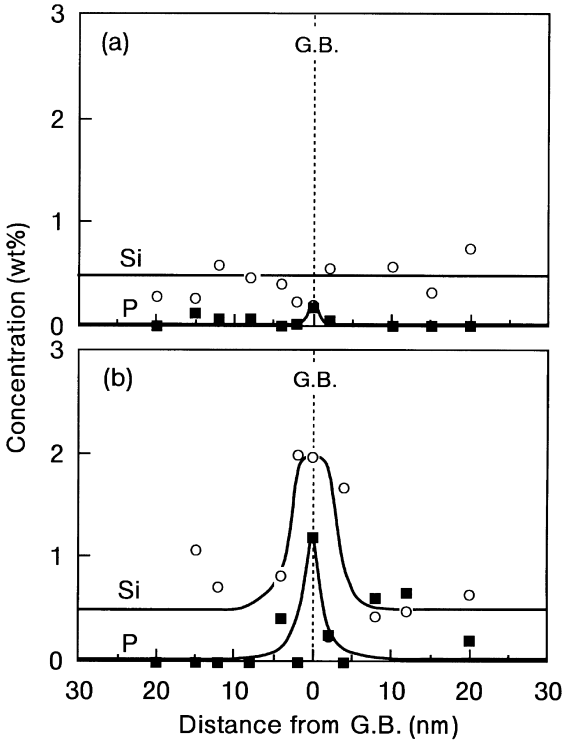

Fig. 7. Si and P profiles near the grain boundary (G.B.) in the thermally sensitized specimen (923 K × 24 h) (a) before and (b) after irradiation to 4 dpa at 723 K.

When the specimens were sensitized at 923 K for 0.5 and 7 h, the RIS of Cr increases with sensitization time. In the case of the specimen sensitized at 923 K for 24 h, the concentration at the grain boundary is not changed by irradiation.

In order to confirm the increase in the degree of sensitization by irradiation, DL-EPR tests were conducted. The reactivation ratio and Cr concentration at grain boundaries before and after irradiation to 4 dpa at 723 K is shown in Fig. 9 for the solution-annealed specimen and the specimen sensitized at 923 K for 0.5 h. The data lie near the curve determined from the thermally sensitized specimen's data (solid line) [12]. The reactivation ratio increases from 12% up to 20% by the irradiation in the specimen thermally sensitized at 923 K for 0.5 h. The surface micrographs after the EPR test are shown in Fig. 10 for the unirradiated and irradiated specimens. Grain boundaries are attacked preferentially in the unirradiated specimen because of the sensitization at 923 K for 0.5 h. After irradiation, grain boundaries are also attacked, but the grooves at grain boundaries are continuous and deeper than those in the unirradiated specimen. This result clearly indicates that the degree of sensitization is increased by irradiation in the specimen. The reactivation ratio is also slightly increased from

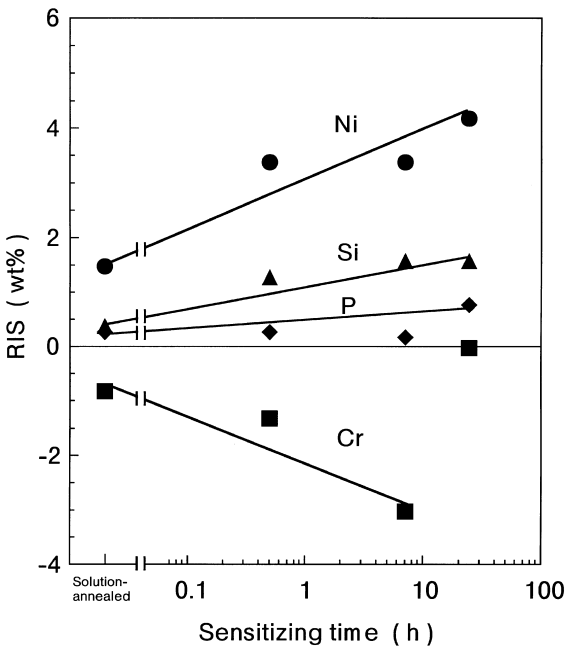

Fig. 8. Radiation-induced segregation (RIS) at grain boundaries caused by the irradiation to 4 dpa at 723 K as a function of thermally sensitizing time of the specimens. RIS : $C^{GB}_{irra} - C^{GB}_{unirra}$.

0.05% to 2% by irradiation to 4 dpa at 723 K in the solution-annealed specimen, as also shown in Fig. 9. However, the solution-annealed specimens before and after irradiation do not show attack of grain boundaries in the EPR test.

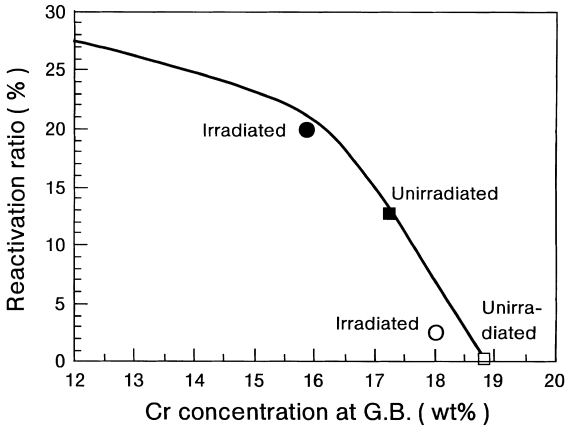

Fig. 9. Correlation between reactivation ratio of DL-EPR tests and Cr concentration at grain boundaries. (■), (●): thermally sensitized at 923 K for 0.5 h; (□), (○): solution-annealed; (■), (□): unirradiated; (●), (○): irradiated to 4 dpa at 723 K and; (——): trend curve of thermally sensitized specimen's data [12].

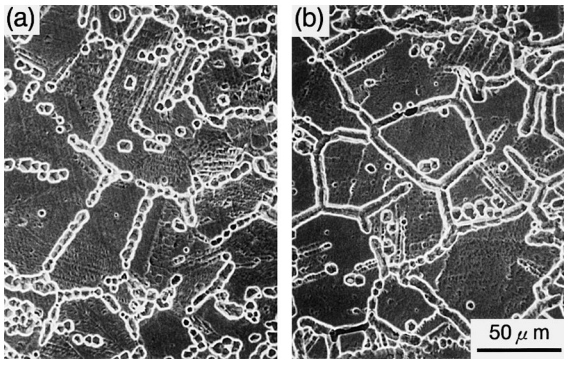

Fig. 10. The surface micrographs after DL-EPR tests in the thermally sensitized specimens (923 K × 0.5 h): (a) before and (b) after irradiation to 4 dpa at 723 K.

4. Discussion

It was seen from the results in Fig. 8 that both radiation-induced Ni enrichment and Cr depletion at grain boundaries are enhanced in the thermally sensitized specimens compared with the solution-annealed specimens. This segregation is attributed to annihilation of radiation-produced interstitials and vacancies into grain boundaries. Hence, the flow of interstitials and vacancies to grain boundaries seems to be relatively larger in thermally sensitized specimens. Microstructural observation was performed in the vicinity of grain boundaries of the solution-annealed and sensitized specimens irradiated to 4 dpa at 723 K. Typical results are seen in Fig. 11. Many dislocation loops are observed in the solution-annealed specimen. There is no significant difference of cluster densities in the vicinity of the grain boundary and the matrix; the density is 5×10^{21} m^{-3}. In the specimen sensitized at 923 K for 24 h, defect-free zones can be seen along the grain boundary, and the cluster density in the matrix is nearly one order of magnitude lower than that in the solution-annealed specimen; the density is 6×10^{20} m^{-3}. Precipitation and coarsening of carbides are not observed at grain boundaries during the irradiation by TEM.

It is well known that loop formation is markedly influenced by impurity atoms of C, P and Si, rather than Cr or Ni, because these impurity atoms act as nucleation sites for loops during irradiation. No change in Si concentration at grain boundaries is found after thermal sensitization treatments [17]. It was reported that Cr carbides picked P atoms as precipitation sites [18]. Therefore, P concentration seems to decrease in areas adjacent to grain boundaries in the sensitized specimens. On the other hand, C atoms form Cr carbides together with Cr atoms. As diffusion of C atoms is much faster than Cr atoms in stainless steels around 923 K [19,20], C concentration is considered to decrease not only near the grain boundaries, but also in the whole grains. Assuming all the carbides to be a spherical-shaped $Cr_{23}C_6$ type (average diameter: 180 nm, average spacing: 150 nm), the C concentration in the matrix is estimated to be about 0.02 wt% in the specimen sensitized at 923 K for 24 h. Since C atoms strongly interact with vacancies [21,22], the reduction of C concentration in the matrix and in the vicinity of grain boundaries is considered to result in an increase in untapped defects, and produces larger flow of point defects into grain boundaries. The effect of C concentration on RIS has been suggested in neutron-irradiated type 348 stainless steels [23]. Fig. 12 shows the correlation between RIS and C concentration after irradiation to 2×10^{25} n/m^2(>1 MeV) at 561 K. C concentration was determined by chemical analysis and RIS was measured by FEG-STEM/EDS method. RIS of Cr, Ni, Si and P are enhanced by lower C concentration. From the above discussion, the enhancement of RIS in thermally sensitized stainless steels can be attributed to radiation-induced point defects having large mobility in the vicinity of grain boundaries, because of a decrease in C near grain boundaries and in the matrix after sensitization heat treatments.

There is no difference between the minimum Cr concentration at the grain boundary before and after irradiation in the specimen sensitized at 923 K for 24 h. Ni, Si and P are, however, segregated at the grain boundary by irradiation, and the RIS for them is somewhat larger than that in the solution-annealed specimen (Figs. 6–8). This fact indicates that the RIS is enhanced in the heavily sensitized specimen. The flux of Cr to grain boundaries during irradiation, J_{Cr}, is expressed by the following equation

$$J_{Cr} = -k_{I-Cr}C_{Cr}D_I\nabla C_I + k_{V-Cr}C_{Cr}D_V\nabla C_V - k_BD_VC_V\nabla C_{Cr},$$

where C is the concentration, D the diffusion constant, k the defect-solute coupling coefficient, I the interstitial and V the vacancies. The first two terms are due to the flow of interstitials and vacancies to grain boundaries, and which make up the inverse Kirkendall effect. The last term is the diffusion of Cr due to the Cr concentration gradient, which is formed by sensitization before irradiation. C_V in this term should be the vacancy concentration during irradiation, not that of the thermal equilibrium. J_{Cr} is determined by a balance between the terms of the inverse Kirkendall effect and the diffusion. Fig. 13 is a schematic illustration of Cr flows near grain boundaries by the inverse Kirkendall effect and the diffusion in a heavily sensitized specimen. Since k_{V-Cr} is larger than k_{I-Cr} in stainless steels, Cr is depleted from grain boundaries during irradiation by the inverse Kirkendall effect. In the heavily sensitized specimen, the initial Cr concentration at the grain boundaries is much lower, and the diffusion term is expected to become

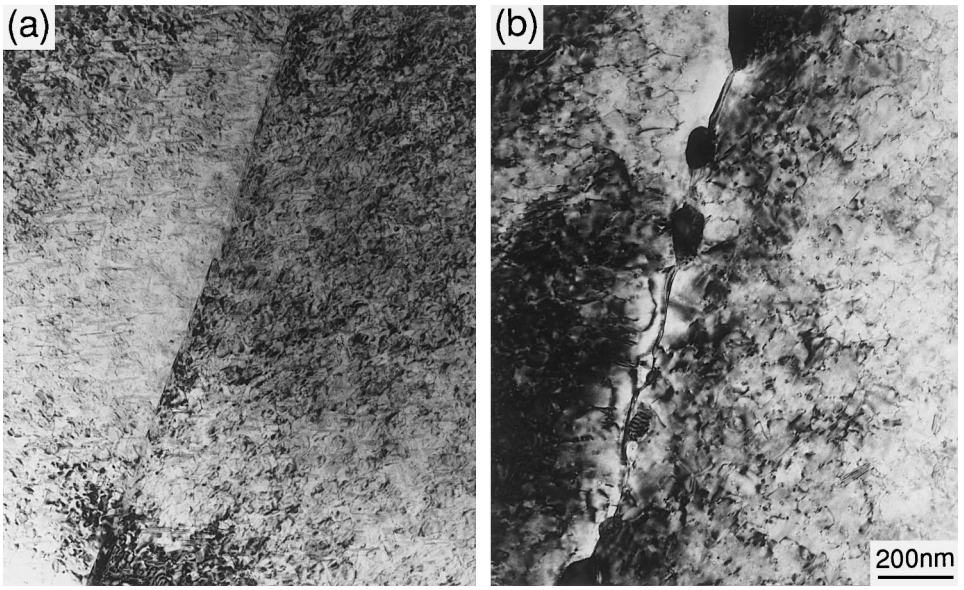

Fig. 11. Damage structures near a grain boundary in: (a) the solution-annealed and (b) thermally sensitized specimens (923 K × 24 h) after irradiation to 4 dpa at 723 K.

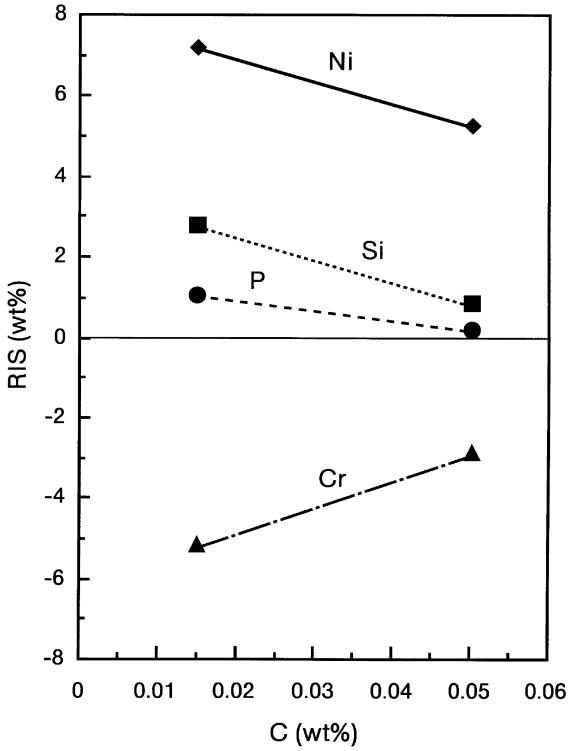

Fig. 12. Correlation between RIS and C concentration in type 348 stainless steels irradiated to 2×10^{25} n/m^2 (>1 MeV) at 561 K. RIS : $C^{GB}_{irra} - C^{GB}_{unirra}$.

large. If the diffusion term exceeds the inverse Kirkendall effect, further Cr depletion dose not occur by irradiation. When the initial Cr concentration at the grain boundaries is not so low as in the specimens sensitized at 923 K for 0.5 or 7 h, the Cr depletion is enhanced by irradiation, because the influence of the inverse Kirkendall effect is larger than that of Cr diffusion.

5. Summary

The radiation-induced segregation (RIS) in thermally sensitized type 304 stainless steel was investigated by He-ion irradiation up to a dose of about 4 dpa at 723 K. The RIS was measured by FEG-TEM/EDS with a nm electron probe. The main results are summarized as follows.

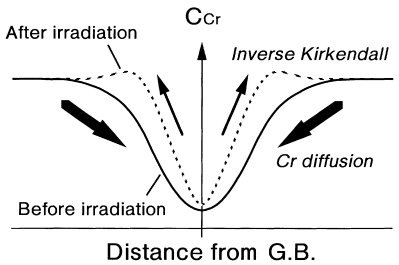

Fig. 13. Schematic illustration of Cr flows near a grain boundary due to the inverse Kirkendall effect and Cr diffusion in a heavily sensitized specimen.

(1) In the specimens thermally sensitized at 923 K, Cr depletion at the grain boundaries were observed, which increased with thermally sensitizing time. Cr concentration at the grain boundary in the specimen sensitized for 24 h fell down to about 11 wt%. No change in Ni and Si concentrations at grain boundaries occurred from the sensitization heat treatments, while P was slightly enriched.

(2) When the solution-annealed specimen was irradiated to about 4 dpa at 723 K, Ni, Si and P were enriched, and Cr was depleted at the grain boundary. The RIS behavior in the sensitized specimens was similar to that in the solution-annealed one. However, although the irradiation dose was the same among the specimens, the RIS of all the elements linearly increased with the logarithm of the thermally sensitizing time, except for Cr in the specimen thermally sensitized at 923 K for 24 h.

(3) The enhancement of RIS in thermally sensitized stainless steels was attributed to radiation-induced point defects having large mobility because of a decrease in C near the grain boundaries and in the matrix after sensitization heat treatments.

(4) It was clarified by the electrochemical potentiokinetic reactivation test (EPR) that the degree of sensitization increased with the progress of Cr depletion at grain boundaries.

(5) Since the diffusion of Cr due to initial Cr concentration gradient near grain boundaries exceeded that of the inverse Kirkendall effect, the Cr concentration at grain boundaries was not changed by irradiation, and the width of the depleted area was narrowed by it in the specimen thermally sensitized for 24 h.

Acknowledgements

The authors are grateful to Dr T. Aoyama of Hitachi Research Laboratory for his support of FEG-TEM/EDS analysis and valuable discussions.

References

[1] K. Nakata, I. Masaoka, J. Nucl. Mater. 150 (1987) 186.
[2] K. Asano, K. Fukuya, K. Nakata, M. Kodama, in: Proceedings of the Fifth International Symposium on Environmental Degradation of Materials in Nuclear Power Systems – Water Reactors, ANS, 1991, p. 838.
[3] M. Kodama, R. Katsura, J. Morisawa, S. Nishimura, S. Suzuki, K. Asano, K. Fukuya, K. Nakata, in: Proceedings of the Sixth International Symposium on Environmental Degradation of Materials in Nuclear Power Systems – Water Reactors, TMS, 1993, p. 583.
[4] S. Kasahara, K. Nakata, A.J. Jacobs, G.P. Wozadlo, K. Fukuya, S. Shima, S. Suzuki, ibid. p. 615.
[5] A.J. Jacobs, G.P. Wozadlo, T. Okada, S. Kawano, K. Nakata, S. Kasahara, S. Suzuki, ibid. p. 597.
[6] K. Fukuya, K. Nakata, A. Horie, in: Proceedings of the Fifth International Symposium on Environmental Degradation of Materials in Nuclear Power Systems – Water Reactors, ANS, 1991, p. 814.
[7] A.J. Jacobs, G.P. Wozadlo, K. Nakata, T. Yoshida, I. Masaoka, in: Proceedings of the Third International Symposium on Environmental Degradation of Materials in Nuclear Power Systems – Water Reactors, TMS, 1987, p. 673.
[8] W.L. Clark, A.J. Jacobs, Proceedings of the First International Symposium on Environmental Degradation of Materials in Nuclear Power Systems – Water Reactors, NACE, 1983, p. 451.
[9] K. Hide, T. Onchi, M. Mayuzumi, K. Dohi, Y. Futamura, Corrosion 51 (1995) 757.
[10] K. Hide, T. Onchi, R. Oyamada, H. Kayano, J. Nucl. Mater. 232 (1996) 30.
[11] A. Kohyama, Y. Kohno, K. Baba, Y. Katoh, A. Hishinuma, J. Nucl. Mater. 191&192 (1992) 722.
[12] O. Okada, K. Nakata, S. Kasahara, T. Aoyama, in: Proceedings of the Eighth International Symposium on Environmental Degradation of Materials in Nuclear Power Systems – Water Reactors, ANS, 1997, p. 743.
[13] G. Cilff, G.W. Lorimer, J. Microsc. 103 (1975) 203.
[14] K. Nakata, O. Okada, Y. Ueki, T. Kamino, J. Elec. Micro. 47 (1998) 193.
[15] R. Katsura, M. Kodama, S. Nishimura, Corrosion 48 (1992) 384.
[16] G.E.C. Bell, T. Inazumi, E.A. Kenik, T. Kondo, J. Nucl. Mater. 187 (1992) 170.
[17] S. Shimanuki, K. Nakata, Tetus To Hagane 83 (1997) 653.
[18] D.V. Edmons, R.W.K. Hoveycombe, in: K.C. Russell, H.I. Aaronson (Eds.), Precipitation Processes in Solids, AIME, 1976, p. 121.
[19] H.K.D.H. Bhadeshia, Met. Sci. 15 (1981) 477.
[20] R.V. Patil, G.P. Tiwari, B.D. Sharma, Met. Sci. Nov. (1980) 525.
[21] K. Nakata, Y. Katano, I. Masaoka, K. Shiraishi, J. Nucl. Mater. 122, 123 (1984) 639.
[22] J.R. Beeler Jr., in: P.C. Gehlen, J.R. Beeler Jr., R.I. Jaffee (Eds.), Interatomic Potentials and Simulation of Lattice Defects, Plenum, New York, 1972, p. 339.
[23] A.J. Jacobs, G.P. Wozadlo, K. Nakata, T. Okada, S. Suzuki, Corrosion 50 (1994) 731.